Nuclear Instruments and Methods in Physics Research A 373 (1996) 358–373

ELSEVIER

NUCLEAR INSTRUMENTS & METHODS IN PHYSICS RESEARCH Section A

The electromagnetic calorimeter of the NOMAD experiment

D. Autiero [a,1], M. Baldo-Ceolin [b], G. Barichello [b], V. Bianchi-Bonaiti [b], F. Bobisut [b], A. Cardini [a,2], P.W. Cattaneo [c], V. Cavasinni [a], C. Conta [c,*], T. Del Prete [a], A. De Santo [a], L. Di Lella [d], R. Ferrari [c], V. Flaminio [a], M. Fraternali [c], D. Gibin [b], S.N. Gninenko [f], A. Guglielmi [b], E. Iacopini [e], A.V. Kovzelev [f], L. La Rotonda [g], A. Lanza [c], M. Laveder [b], C. Lazzeroni [a], M. Livan [c], M. Mezzetto [b], D. Orestano [c,3], F. Pastore [c], E. Pennacchio [c,4], R. Petti [c], G. Polesello [c], G. Renzoni [a], A. Rimoldi [c], C. Roda [a,1], A. Sconza [b], C. Sobczynski [d], M. Valdata-Nappi [g], M. Vascon [b], V. Vercesi [c], L. Visentin [b], S.A. Volkov [f]

[a] *Dipartimento di Fisica, Università di Pisa and INFN, Sezione di Pisa, Pisa, Italy*

[b] *Dipartimento di Fisica, Università di Padova and INFN, Sezione di Padova, Padova, Italy*

[c] *Dipartimento di Fisica Nucleare e Teorica, Università di Pavia and INFN, Sezione di Pavia, Pavia, Italy*

[d] *CERN, Geneva, Switzerland*

[e] *Dipartimento di Fisica, Università di Firenze and INFN, Sezione di Firenze, Firenze, Italy*

[f] *Institute of Nuclear Research, INR, Moscow, Russia*

[g] *Dipartimento di Fisica, Università della Calabria and INFN, Gruppo collegato di Cosenza, Cosenza, Italy*

Received 13 November 1995

Abstract

A description is given of the NOMAD electromagnetic calorimeter, consisting of 875 lead–glass counters read out by two-stage photomultipliers and a low noise electronic chain. The detector operates in a 0.4 T magnetic field transverse to the counter axis. The paper discusses the design criteria, the lead–glass characteristics, the properties of the read out chain and provides a summary of the calorimeter performance.

This paper is dedicated to the memory of Giorgio Fumagalli from Pavia and Toni Cavestro from Padova, in whom we lost outstanding colleagues and good friends.

1. Introduction

1.1. The NOMAD experiment

The aim of the WA-96 experiment (NOMAD, for Neutrino Oscillation MAgnetic Detector) [1] is to observe neutrino oscillations between ν_μ's (or ν_e's) and ν_τ's. The experiment looks for the appearance of ν_τ's in the CERN neutrino beam consisting mostly of ν_μ's, with a negligible ν_τ content. The ν_τ's are to be observed through their charge current interactions producing τ^-'s. The τ^-'s in turn are to be observed through their leptonic decays into $e^-\bar{\nu}_e\nu_\tau$ and $\mu^-\bar{\nu}_\mu\nu_\tau$ and through their hadronic decays such as $\pi^-\nu_\tau$, $\rho^-\nu_\tau$, $\pi^+\pi^-\pi^-\nu_\tau$. The experiment is sensitive to 78% of the τ branching ratio.

NOMAD uses a technique which distinguishes τ decays from ν_μ and ν_e charged and neutral current interactions through a series of cuts on kinematical variables such as missing p_T, and angular correlations between the hadronic vector, the missing p_T and the leptonic or hadronic decay products of the τ.

A layout of the NOMAD detector is shown in Fig. 1.

For a precise determination of the hadronic vector, a very accurate measurement of the momentum of charged and neutral hadrons as well as of photons is required.

The momentum of charged particles is measured by their curvature in the 0.4 T magnetic field, using 147 drift planes. The drift-chamber walls provide at the same time the target material for neutrino interactions.

The electron and photon energies are measured in an electromagnetic calorimeter which is the subject of this paper. The calorimeter is preceded by a preshower consisting of a 9 mm thick lead plate followed by a plane of vertical and a plane of horizontal proportional tubes. The preshower is used for e/π discrimination through the early shower devel-

* Corresponding author.

[1] Now at CERN.

[2] Now at UCLA.

[3] Now at the University of Roma 3, Italy.

[4] Now at the University of Urbino, Italy.

PII S0168-9002(96)00070-8

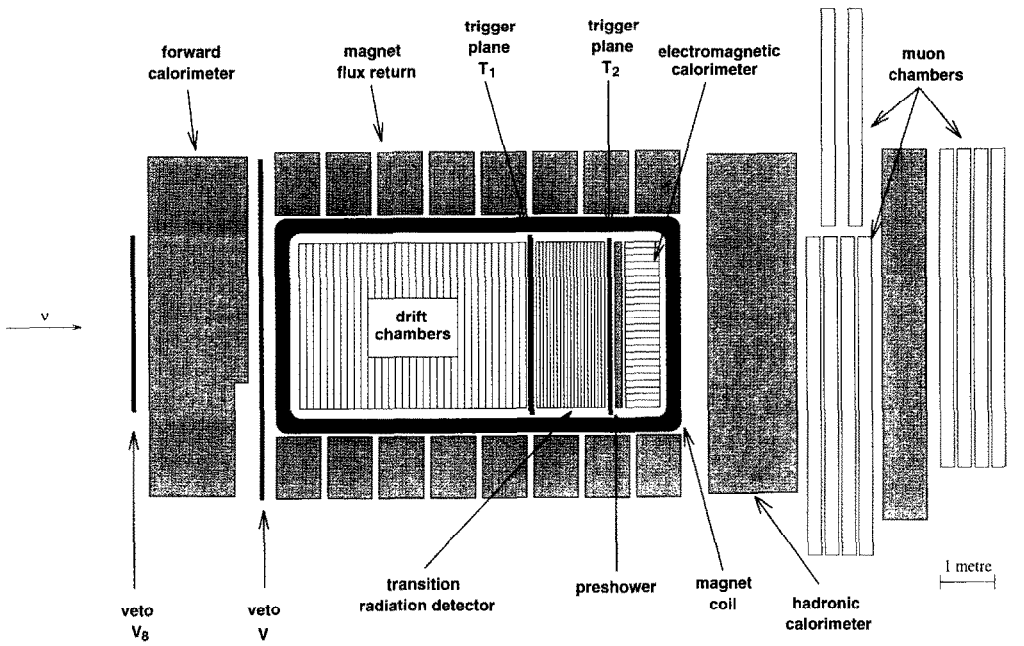

Fig. 1. A schematic side view of the NOMAD detector.

opment technique and for better spatial localization of the photons that convert in the lead.

Further discrimination between electrons and pions is provided by a 9 module Transition Radiation Detector (TRD).

All the above detector components are placed inside the magnet that provides a 0.4 T field over a $7.5 \times 3.5 \times 3.4$ m^3 volume.

An iron-scintillator hadron calorimeter [2] placed outside the magnetic volume follows the e.m. calorimeter and is itself followed by a muon spectrometer. Finally three scintillator planes are used, the first one placed upstream of the detector, to veto muons accompanying the neutrino beam, the other two placed one after the drift chambers and one after the TRD to provide a charged particle trigger.

1.2. The electromagnetic calorimeter

The task of the electromagnetic calorimeter is to provide a precise measurement of the energy, position and direction of the electromagnetic showers induced by electrons and photons. A large dynamic range is required, in order to detect energy depositions from less than 100 MeV to above 100 GeV. A π/e rejection of the order of 10^3 is also needed. A lead–glass detector has been chosen for its excellent energy resolution and response uniformity.

The calorimeter consists of 875 lead–glass Cherenkov counters of TF1-000 type [3], 19 radiation lengths deep and with a rectangular cross section of 79×112 mm^2.

The direction of the $B = 0.4$ T magnetic field is perpendicular to the counter axis, imposing severe constraints on the choice of a light detection system which can fully exploit the lead–glass properties. With a magnetic field perpendicular to the tube axis no photomultiplier would be able to operate, while other devices do not offer adequate signal amplification, or were not yet at a mature enough development stage to match the experiment time scale.

To overcome these problems, the face of the lead–glass block coupled to the light detector has been cut at 45° (Fig. 2) with respect to the counter axis and to the magnetic field direction. Although multi-stage PMs would still

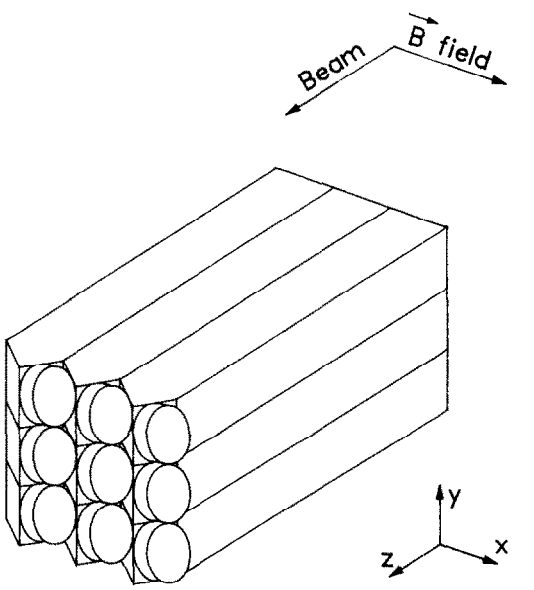

Fig. 2. Schematic view of some lead–glass counters with phototetrodes.

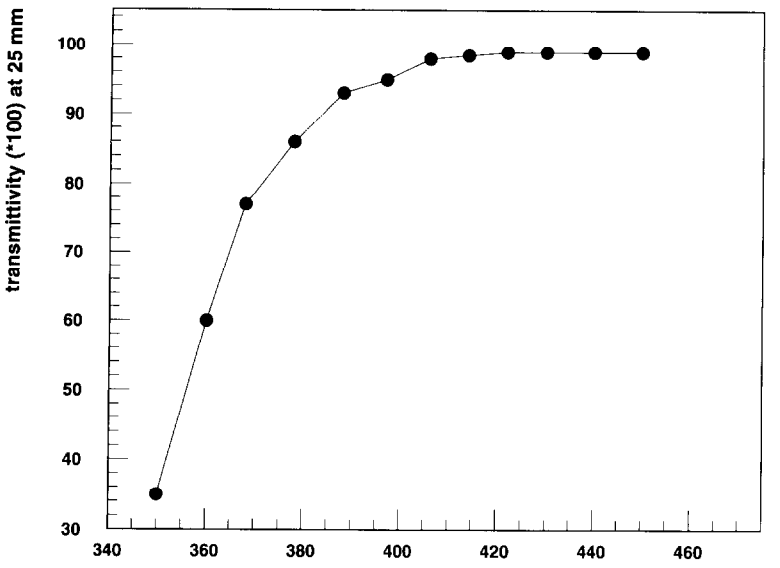

Fig. 3. Glass transmittivity.

be in a critical operating region, single stage PMs (triodes) – already proposed [4] and used [5–7] for operation in a magnetic environment, albeit at lower tilt angles – can cope with such a field orientation. However the triode gain (typically below 10 in these conditions) does not allow an acceptable signal to noise ratio, given the presently reachable quantum efficiency (QE) values.

Recently two-stage photomultipliers (tetrodes) have been developed, which show an angular dependence similar to that of the triode, with a typical gain of 40 in the operating conditions of NOMAD. Therefore the electromagnetic calorimeter has been equipped with a light detection system based on tetrodes, whose diameter (77 mm) provides optimal compromise between granularity, cost and system complexity.

The signal is amplified and shaped by a low noise electronic chain allowing for a dynamic range of about 5×10^3. In order to compensate for the variation in gain among tetrodes, a solution based on the shaping amplifier stage has been developed to equalize the signal. In addition, a fast signal is provided for time measurement with a resolution of a few nanoseconds for energy depositions larger than 1 GeV.

This paper is organized as follows. Section 2 discusses the criteria for the choice of the lead–glass and its parameters. Section 3 describes the tetrode structure, the assembly of the calorimeter counters and the general properties of the photomultipliers. Section 4 addresses the study of the tetrode behaviour in a magnetic field, and the choice of operating conditions. Section 5 covers the design and performance of the electronic chain, and Section 6 summarizes some results on the detector performance.

2. The lead–glass counters

As explained in Section 1.2, to reach the best photoelectron yield inside the magnetic field, 77 mm diameter phototetrodes oriented at 45° with respect to $\boldsymbol{B}$ are an optimal choice: this dictates the cross section of the lead–glass blocks to be 79×112 mm^2. With this choice the geometric shape of the glass blocks has a reduced symmetry: the transverse horizontal and vertical sizes are different and the depth is not constant across the calorimeter surface. Moreover the read out detector is not symmetric with respect to the block axis. These features could in principle spoil the calorimeter response and cancel the advantages of the use of a homogeneous medium. The size and shape of the blocks affect both the physical development of the shower and its light collection efficiency. To finalize the design of the blocks a Monte Carlo (MC) study was performed, in which the shower development was simulated down to the Cherenkov threshold energy. The simulation also included a detailed description of the production, propagation through the blocks and conversion of the Cherenkov photons. This study allowed to estimate to about 25% the signal reduction due to the tilt angle of the photodetector. The signal amplitude increases when reducing the block length due to the finite glass transparency. For instance, changing from 22 to $20X_0$, an increase of 6% in the output signal is expected and it was verified at a 6 GeV e^- test beam. On the other hand the block should be long enough to contain the shower development and to allow a proper randomization of the light reaching the photo-detector. For instance, the mean energy of electrons from τ^- decays is expected to be about 10 GeV, with a distribution peaking at a few GeV; the mean energy for electrons coming from ν_eCC events is around 30 GeV; with a $19X_0$ depth, the longitudinal leakage is 0.6% for a 5 GeV and 1.6% for a 50 GeV shower.

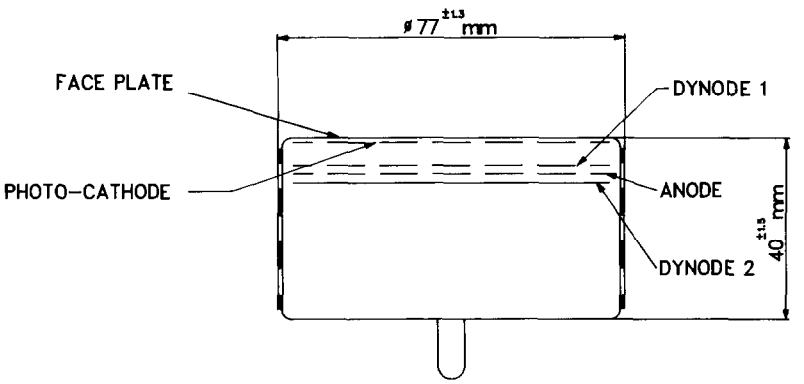

Fig. 4. Schematic view of the R2186-01 tetrode.

The MC calculations showed that a depth of $18–20X_0$ would provide the best performance in terms of signal uniformity as a function of the shower impact position and angle as well as in terms of energy resolution.

The lead–glass used is TF1-000, similar to that used in the GAMS detector [8]; its composition by weight is: 52.3% PbO, 40.2% SiO_2, 7% K_2O, 0.5% As_2O_3, and its radiation length is $X_0 = 26.8$ mm. The longitudinal dimension of the blocks is 500 mm, corresponding to about $19X_0$.

The internal transmittance $T_i(\lambda)$ has been measured on small samples at the Stazione Sperimentale del Vetro, Murano: referred to a thickness of 25 mm, $T_i \geq 0.99$ for $\lambda >$ 410 nm: see also Fig. 3. During the mass production T_i was required (and checked) to be larger than 0.76 at $\lambda = 370$ nm and larger than 0.97 for $\lambda > 410$ nm.

Most of the blocks were machined with a precision better than 100 μm in the transverse dimension. This allowed to wrap them with a 100 μm thick sheet and stack the 875 blocks in 35 rows of 25 elements each, thereby minimizing the dead space between adjacent counters. Stacking a few rows and loading them with an extra weight corresponding to the maximum load in the full calorimeter, resulted in a few percent variation of the light yield, depending on the wrapping. The best result, about 1% variation between load and no-load measurements, was obtained with the white diffusing Tyvek[5], which was adopted as the final wrapping. The whole calorimeter, including the lead–glass blocks, the phototetrodes with pre-amplifiers, the distribution cards (described in Section 5.4) and the cables was assembled in a 3×3 m^2 stainless steel frame.

3. Phototetrode description and properties

3.1. Phototetrode design

The phototetrodes (type R2186-01) were supplied by Hamamatsu. The layout is schematically shown in Fig. 4.

[5] Produced by Dupont de Nemours.

When light hits the bialkali photocathode, the generated photoelectrons are accelerated by the electric field towards dynode 1, which consists of a fine mesh electrode designed for operation in a magnetic environment. The secondary electrons which are produced are then accelerated towards the anode, itself a mesh electrode, and most of them traverse it and hit dynode 2 where further electron multiplication occurs. The resulting electrons are finally collected by the anode as output signal.

The inter-dynode voltage must not exceed 600 V and the maximum voltage difference between cathode and ground (anode) is 1250 V.

3.2. Mechanical assembly

Due to the confined space allowed for the detector inside the magnet, a compact mechanical assembly had to be adopted.

The tube position is constrained by an aluminium frame glued onto the lead–glass back-face, and also supporting two Light Emitting Diodes (LEDs) used for monitoring purposes [9]. A circular PCB of the same tetrode diameter (77 mm) houses both the high voltage divider and the preamplifier, with an additional space occupancy of only 15 mm along the tube axis. A cylindrical copper cover, 63 mm long and 0.2 mm thick, which allows the routing of voltage and signal cables, contains the whole assembly, and protects the preamplifier from external pick-up and disturbance induced by the LED pulsing.

In order to optimize the light yield, several solutions have been tested for the optical coupling of the phototetrode to the lead–glass. Interposition of an elastomer or silicon grease increases the signal by a factor of 1.5–1.8, but does not guarantee stability of the response with time. The best result has been obtained by using an epoxy resin (EPOTEK 301-2) with a refraction index intermediate between that of lead–glass ($n = 1.648$ at 589 nm) and the one of the photomultiplier face-plate ($n = 1.484$ at 589 nm), with an average increase in response of a factor of about 2.5 compared to

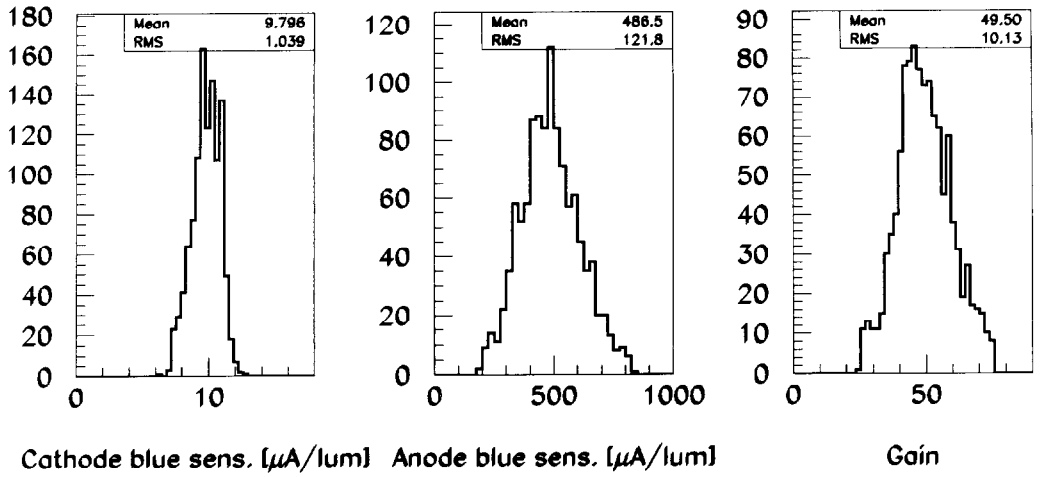

Fig. 5. Tetrode response parameters for the full sample used in the experiment.

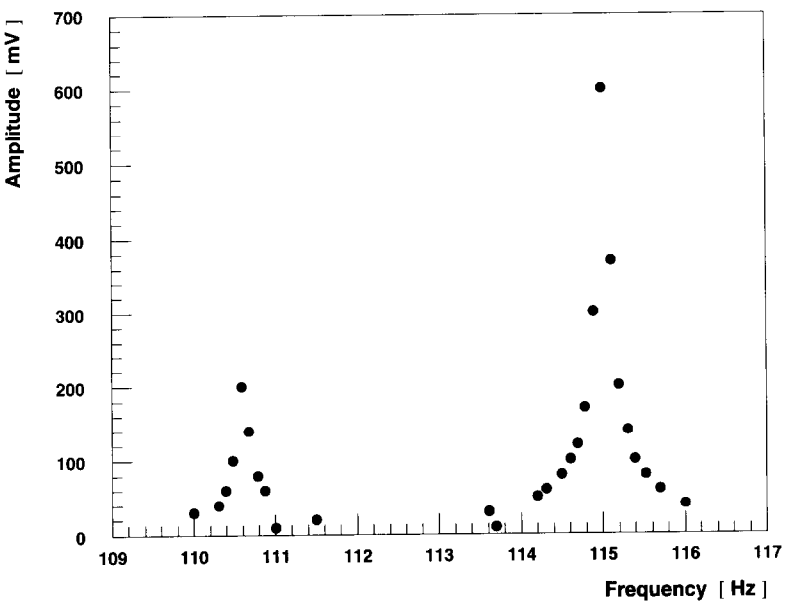

Fig. 6. Microphonic effects in presence of two resonance frequencies at $B = 0$ T.

a pure mechanical contact. In addition, the gluing provides excellent mechanical stability and protection against humidity, contributing to the time stability of the response.

3.3. General parameters

The R2186-01 photocathode is characterized by a low dark current (<1 nA) and good QE, with a maximum around 20–25% in a spectral region well matched to the lead–glass transmitted light.

Fig. 5 shows the distributions of gains (at $B = 0$ T and a supply voltage of 1 kV) and of cathode and anode blue sensitivities, as given by the manufacturer[6], for the whole sample of tetrodes installed in the calorimeter. These parameters have substantially improved with respect to the previous version of the tetrode (R2186), following close contacts with Hamamatsu during the initial phase of the project. In particular the cathode blue sensitivity, closely related to QE, strongly contributes to the energy resolution of the detector.

[6] The luminous sensitivity is defined by the manufacturer as the output current obtained from the cathode or anode divided by the incident luminous flux (in lumen) from a tungsten lamp at a distribution temperature of 2856 K. The blue sensitivity is obtained when a blue filter, whose spectral transmittance peaks at 420 nm, is placed in front of the PM in the same conditions.

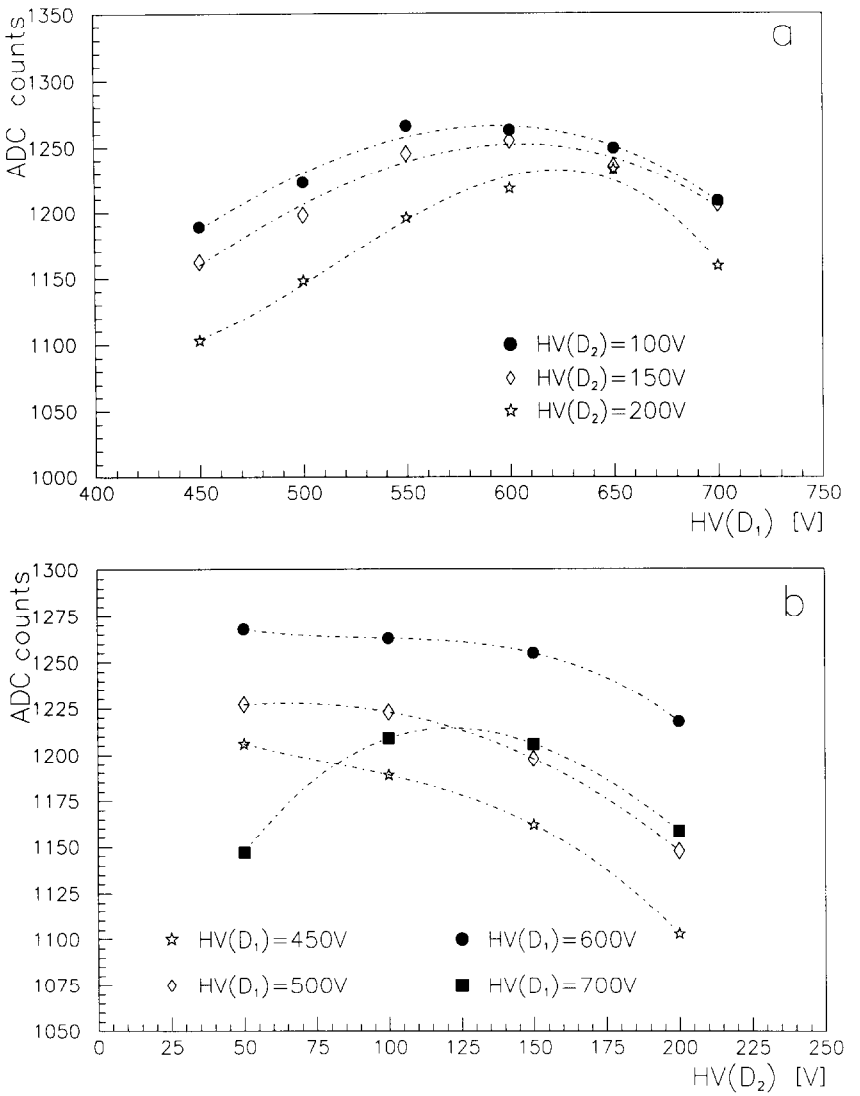

Fig. 7. Study for the tetrode voltage divider. The optimization was performed at $B = 0.4$ T and $\phi = 45^{\circ}$. (a) Signal vs. dynode 1 voltage, for fixed dynode 2 setting; (b) signal vs. dynode 2, for fixed dynode 1 setting. The cathode voltage is 1000 V.

Together with an average gain of 50 (reduced by less than 20% in the operating conditions of the experiment), this results in an excellent signal to noise ratio.

The rather large spread of the anode blue sensitivity, combined with the cell to cell fluctuations of the light yield to the photocathode, disfavours a signal equalization based on HV adjusting. Such a method would in fact cause some PMs to work around 200–300 V, a critical operating region in the presence of a magnetic field. In particular, below 600 V the response to electrons is no longer tracked accurately by the monitoring LEDs. To overcome the problem, the gain adjustment has been implemented through a gain regulation of the shaping amplifier stage, as explained in Section 5.2.

3.4. Microphonic effects

Due to their internal structure, the photodetectors show microphonic effects [4,10], mainly relevant in the range of frequencies between 0 and 900 Hz. These are caused by vibrations of the membranes inside the tetrode (the dynodes and the anode), which can generate electrical signals due to capacitive effects, amplified by the read out chain. Acoustic noise is important if the unipolar output of the shaping stage is used (see Section 5.2).

To study the problem sounds were generated by means of a loudspeaker controlled by a precision frequency synthesizer. A complex spectrum of resonances was found, which included several fundamental frequencies and their higher harmonics. The resonances, which show a pure sinusoidal

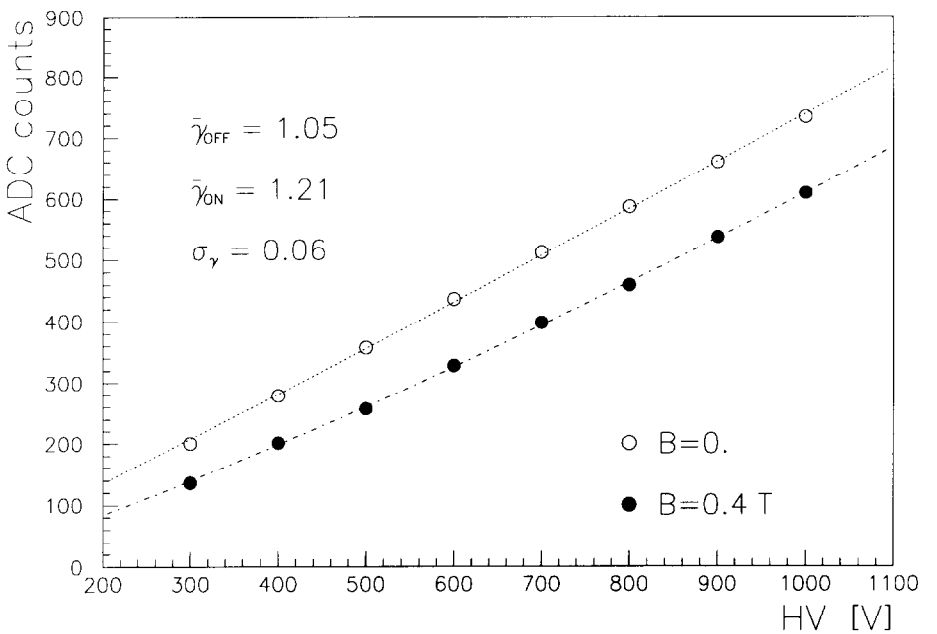

Fig. 8. Relative gain-voltage dependence as measured on a sample of 15 tetrodes.

shape, are very narrow and, in the absence of a magnetic field, may have an amplitude up to 2.5 V, at an operating voltage of 800 V. As an example, the output amplitude for two close resonances is shown in Fig. 6.

However, in the presence of a magnetic field, the acoustic noise is damped in amplitude by about a factor of 10. Moreover the bipolar shaping used in the experiment acts as a filter, suppressing this low frequency component.

4. Phototetrode performance in a magnetic field

The tetrode behaviour in a magnetic field has been studied under several conditions. To determine the response integrated over the whole photocathode surface, the PM, placed in a test magnet, was coupled to a light guide illuminated by a LED. Furthermore, results are available for the whole detector inside the experimental magnet, where all the tetrodes are coupled to the lead–glass counters. In this respect, it has to be remarked that the response to LED light closely follows the one to electrons, as extensively studied in beam tests.

In both configurations either the light guide or the lead–glass block act as light mixers, thus preventing the detection of local response variations over the photocathode surface. In order to study local non-uniformities, the tetrode face plate has been scanned by a nearly point-like source directly placed in front of it.

In the following, results on the integrated response will be presented first, and will be followed by a discussion on the variation in the response of the tetrode across its face.

4.1. Integrated response

4.1.1. Choice of operating conditions

To optimize the signal output, the voltage divider ratio has been studied in the operating conditions of the experiment, namely $B = 0.4$ T at a tilt angle $\phi = 45°$ of the tube axis with respect to the field direction, in a test magnet. The two dynodes D_1 and D_2 were independently fed with high voltage, at a fixed cathode supply. The results are shown in Fig. 7. For HV(cathode) = 1000 V the maximum signal is found for $HV(D_1) = 600$ V and $HV(D_2) = 100$ V with respect to ground, corresponding to a 4 : 5 : 1 ratio for the interstage voltages. In order not to approach the maximum potential difference specified for the dynodes, the adopted voltage divider (see scheme in Fig. 13) provides a 2.6 : 3.1 : 1 ratio, different from the ones suggested by the manufacturer for standard operation. Such a configuration, while keeping a high gain, assures a safe operation at the working point of 800 V chosen for the experiment.

The gain dependence on the applied voltage is almost linear, only varying slightly as a function of the magnetic field. Fig. 8 shows the gain-voltage relationship, which can be parametrized as $G \propto V^\gamma$. In the working conditions of the experiment, $\gamma = 1.2$, approaching 1 for non-magnetic operation. The average gain in a $B = 0.4$ T field and a tilt angle $\phi = 45°$ is $G = 40$ at HV = 800 V.

4.1.2. Field dependence

As a function of the ϕ angle, the tetrode response exhibits the typical dependence shown in Fig. 9. This behaviour has been found to be almost independent of the applied HV, in the range 700–1000 V. The relative output is maximum

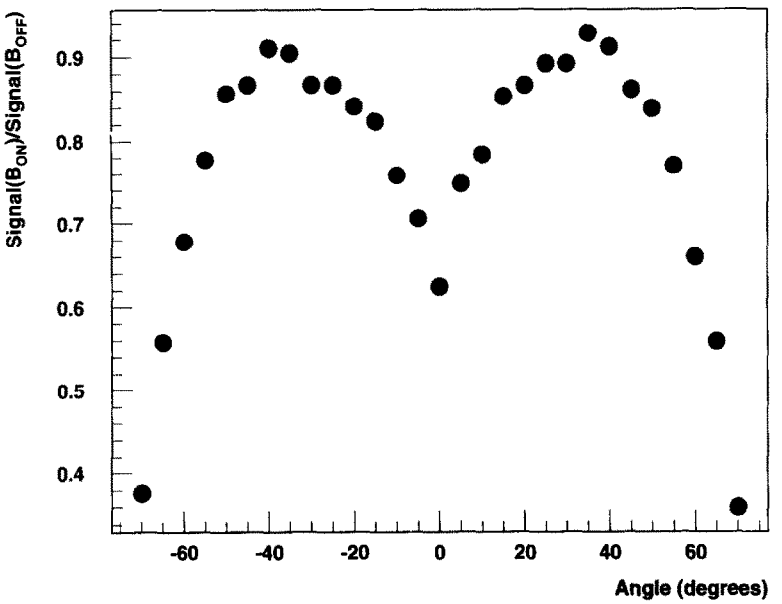

Fig. 9. Average angular response in a 0.4 T magnetic field, normalized to the zero-field situation.

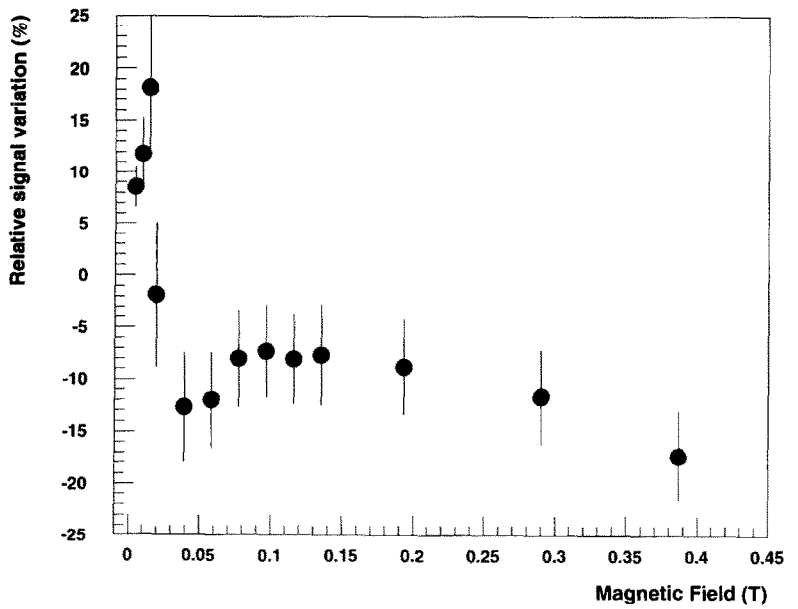

Fig. 10. Response variation measured in the experimental magnet as a function of B intensity, normalized to the value at $B = 0$ T. The error bars show the RMS of the distributions for the full tetrode sample installed in the detector.

around $\phi = 30°$, and is still above 80% for $\phi = 45°$ showing an improvement over the performance of triodes used in previous experiments [5,7].

The response as a function of the field intensity at $\phi = 45°$ has been measured in the range 0 – 0.4 T for the whole tetrode sample installed in the calorimeter (Fig. 10). An increase is observed for low field values followed by a sharp decrease up to 0.05 T and a second maximum, followed by a slow decrease above 0.15 T. A similar feature has already been observed in triodes operating in an axial field [5] and it was attributed to the internal geometry of the photodetector. In the case of the R2186-01 tetrode the low field response behaviour can probably be explained by a field-dependent screening effect from the mesh dynode 1. In general, part of the secondary electrons hit the mesh dynode grid and cannot reach dynode 2. For particular field values the transmission efficiency to the next dynode may improve, resulting in an increase in gain. For each tetrode, the response is almost insensitive to the field non-uniformities in direction ($\pm 1°$) and intensity ($\pm 5\%$) existing in the magnetic volume of the

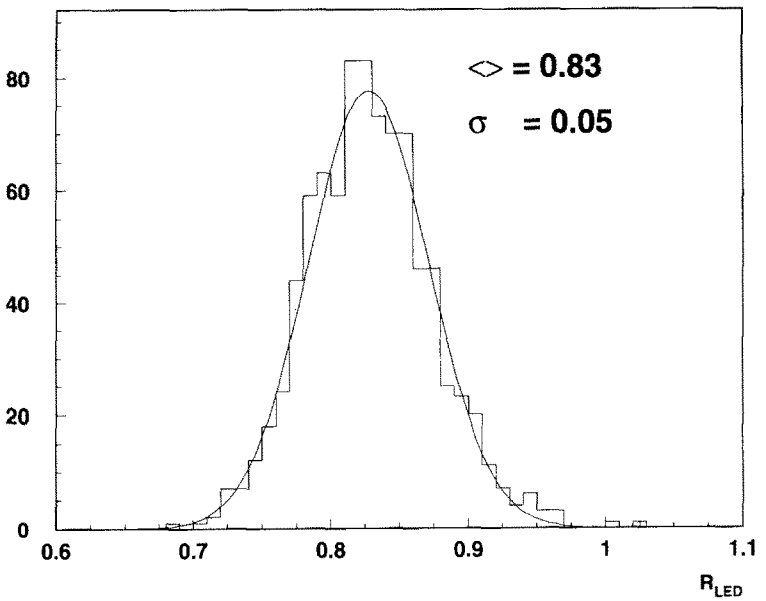

Fig. 11. Distribution of the relative response at $B = 0.4$ T and $\phi = 45°$ for the full tetrode sample.

experiment (Figs. 9 and 10).

For the whole tetrode sample operating in the experimental magnet, the response at $B = 0.4$ T relative to $B = 0$ T is shown in Fig. 11. Since the signal is almost unaffected by the existing field non-uniformities, the spread in the distribution is to be attributed to differences in the behaviour of individual tetrodes. This limits the accuracy of a response equalization performed in the absence of a magnetic field.

4.2. Local response

In order to better understand the origin of the integrated effects on the tetrode response discussed above, a LED of 1 mm^2 spot size was moved over the surface of the photocathode. First a measurement in the absence of magnetic field by means of an X–Y scanner capable of an accuracy of 0.1 mm showed the photocathode response to be uniform within $\pm 2\%$. The PM was then placed inside a magnet and the response to the LED light was measured in a grid of positions in steps of 8 mm.

The local response variation with respect to the output at zero field is displayed in Fig. 12 for three different ϕ angles of the tube axis with respect to the field direction, at $B = 0.4$ T. For $\phi = 0°$, the decrease in response induced by the magnetic field is observed to be uniform over the photocathode surface (slightly larger than 30%, in accordance with the observed integrated response), apart from a further loss at the outer edges. When the tube axis is at non-zero angles with respect to the field direction, a blind region appears on the photocathode, approximately of a quarter moon shape (Fig. 12d), whose extension grows as a function of the tilt angle ϕ. However, the response in part of the efficient region becomes larger than the one at $B = 0$ T and increases with the ϕ angle at least up to 60°. The combined contribution of these two opposite effects accounts for the integrated angular response shown in Fig. 9, in particular for the maximum at 30° and the slow variation of the global response up to about 60°. However, at non-zero tilt angles, the uniformity of the photocathode is strongly affected.

While for the local increase of efficiency a clear explanation could not be found, the appearance of the inefficient region can be understood by means of a simple model. In a magnetic field of 0.4 T and an electric field of 400 V/cm inside the tetrode, the photoelectrons emitted by the photocathode follow spiral trajectories along the magnetic field lines with a radius of the order of a fraction of a millimetre. In general, for sufficiently high intensity of the magnetic field, the photoelectrons can be considered to a good approximation as moving along the field lines. Since part of the photocathode is not covered by the projection of the anode along the field lines, the photoelectrons originating in this area never reach the anode. This gives rise to the blind region.

No significant dependence of the response variation on the LED light wavelength was found (yellow, red, green and blue LEDs were used). The inversion of the magnetic field direction was found not to change the location of the inefficient area and the reduction of the integrated signal.

5. Readout electronics

The electronic chain for each of the 875 channels, schematically shown in Fig. 13, is composed of a charge preamplifier, followed by a shaper and a peak-searching ADC with a resolution of 12 bits.

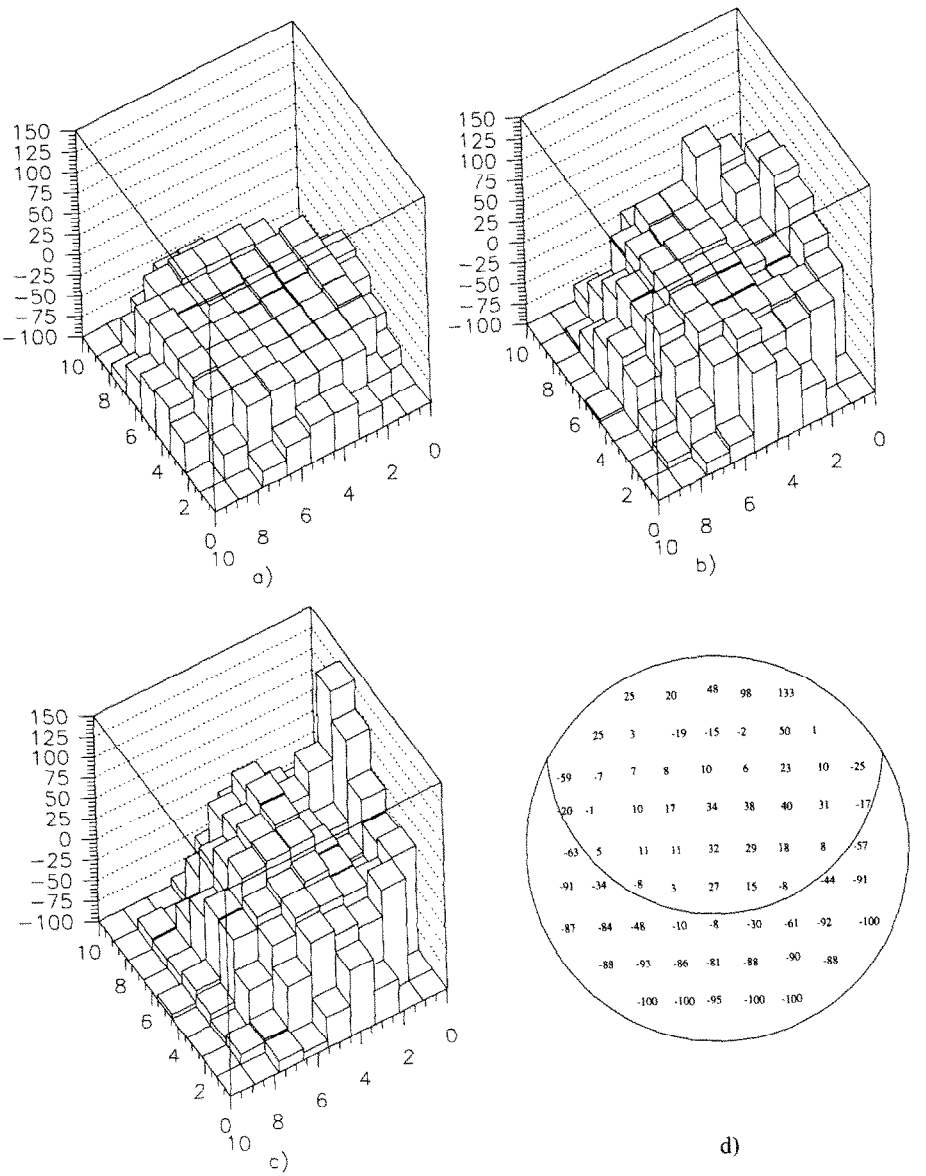

Fig. 12. Map of the photocathode scan. The local response variation (in percent) with respect to $B = 0$ T is shown for $B = 0.4$ T at three different tilt angles: (a) $\phi = 0°$, (b) $\phi = 30°$, (c) $\phi = 45°$, (d) the boundary of the inefficient area is shown for $\phi = 45°$.

The preamplifier and the shaper designs are based on the read out chain developed for the Delphi lead–glass calorimeter [10,11], modified to fit the NOMAD requirements. In particular the dynamic range has been extended and a variable amplification has been introduced at the shaper stage. To achieve a good signal to noise ratio, particular care has been devoted to minimizing the intrinsic electronic noise. The slight increase in noise due to the higher input capacitance of the R2186-01 tetrode with respect to the triode adopted by Delphi is largely compensated by its improved gain.

5.1. Charge preamplifier

In correspondence to the maximum energy to be detected, a released charge of 900 fC is expected in the calorimeter. In order to include this value into the linearity region, two operational amplifiers were adopted in the final stage instead of two discrete transistors. The dual op amp AD827 was chosen for its small power requirements and the capability of providing up to 30 mA output current. With this final stage the linearity region extends to 3000 fC and the power dissipation is 220 mW/ch.

The preamplifier is AC coupled to the tetrode, to avoid the shifting of the working point of the JFET due to the

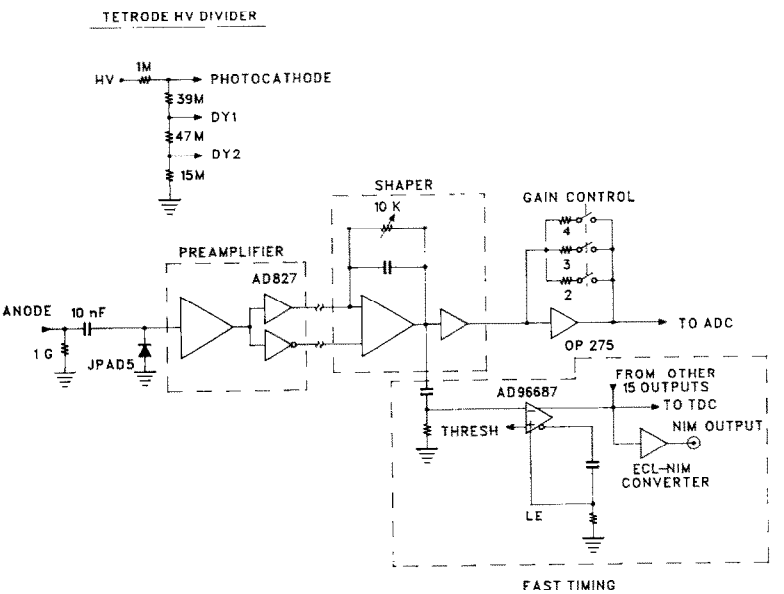

Fig. 13. Layout of the electronic chain. Only the changes implemented with respect to Ref. [8] are drawn in detail, together with the voltage divider.

voltage drop on the anode resistance caused by the tetrode dark current. The value of the anode resistance is as high as 1 GΩ to reduce its contribution to the noise. The input is protected against sharp signals spikes caused by variations of the tetrode high voltage with a Siliconix JPAD5 diode, which has a maximum reverse current of 5 pA and a reverse capacitance of 1.5 pF.

The typical anodic capacitance of the R2186-01 tetrode is 40 pF. A good matching is provided by the JFET IF1320. A test performed on 9 channels in a test beam has given good results in the noise performance (see Section 5.5.1).

A test signal for the whole electronic chain is fed to all the preamplifiers through the distribution cards placed on the calorimeter (see Section 5.4). The signal is formed by a variable square pulse generator implemented in a double VME module. The amplitude, frequency and duty cycle of the square wave are manually and computer programmable and steps of square pulses can be generated. A digital selection on the distribution cards allows the enabling of 8 channels or multiples of 8 at a time.

5.2. Shaper

The shaper is composed of three stages: the first is the receiver for the differential input signal, with a small integration constant; the second is the integration stage to obtain the final waveform, coupled through a pole-zero circuit to the first stage; the final stage is a sample-and-hold circuit with unitary gain.

To obtain the response regulation (see Section 3.3) a 10 kΩ multi-turn trimmer was used in the first stage. The small variation of the integration time constant does not alter the final response of the shaper.

A further amplification was introduced to avoid the shaper non-linearity for output signals exceeding 7 V at the supply voltage of ±12 V. The final amplifier (an op amp OP275) is designed to obtain an amplification factor of 2,3 or 4 remotely selectable. The factor 2 is used in standard operation and assures the linearity of the system up to 10 V, the range of the ADC, whereas the larger amplification factors can be used for calibration purposes to detect signals close to the pedestal (as those due to muons).

The output shape of the signal can be bipolar or unipolar, selectable with a jumper. The bipolar signal was preferred to filter the acoustic noise due to mechanical vibrations of the tetrode electrodes, as discussed in Section 3.4. The shaping time for the bipolar signal is 1.4 μs.

5.3. ADC

The ADC is of the peak-searching type. This technique was preferred to the more common charge-integrating one in order to get a high input impedance (10 kΩ) and to avoid the necessity of critical timing of the gates.

It uses a 12-bit integrated circuit, Burr-Brown ADS7800, with 3 μs conversion time. The gate is a NIM signal whose falling edge enables the peak search, and must precede the analog signal peak by at least 600 ns. The peak-searching circuitry is active for 2.2 μs, after which the conversion of the recorded peak value begins.

The integral linearity was evaluated with a statistical method, based on the conversion of signals whose variable amplitude was randomly distributed within the ADC range of 10 V. For each of the 64 channels of the 14 Fastbus

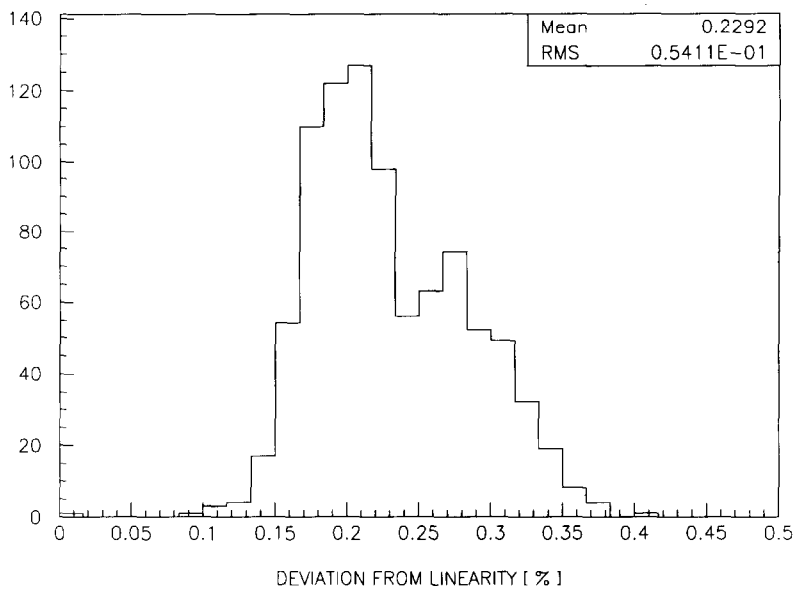

Fig. 14. Distribution of the maximum deviation from linearity for all the ADC channels.

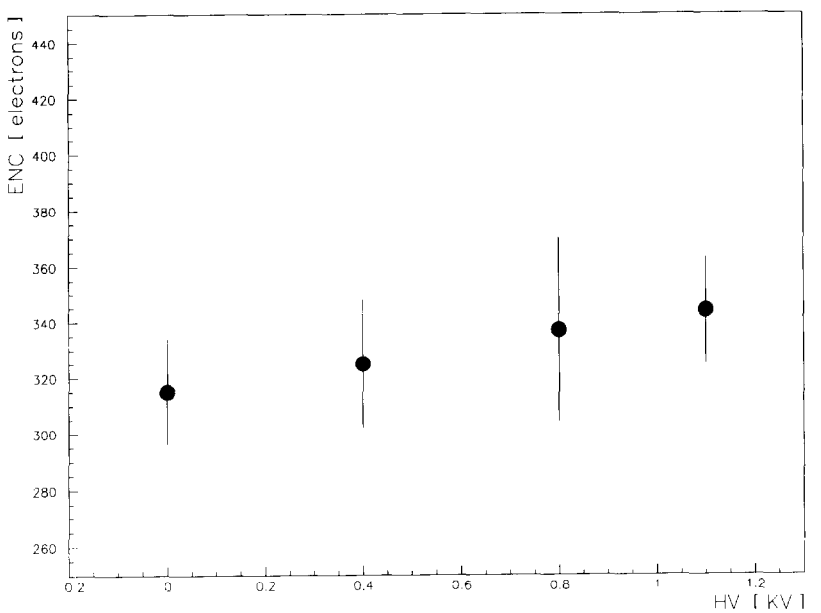

Fig. 15. HV dependence of the electronic noise (ENC) for a sample of 9 channels.

boards the content of the 4096 ADC steps was obtained. From these distributions the maximum deviations from linearity were deduced. In Fig. 14 the distribution of the maximum deviation from linearity for all the channels is plotted. The ADCs are linear within 0.3%.

5.4. Mechanical layout

The charge preamplifier is a hybrid circuit of 2×2.5 cm^2, located together with the voltage divider on a circular PCB soldered directly on the tetrode pins. To simplify the cabling, 28 distribution cards are placed over the calorimeter face equipped with the photodetectors, each supplying the low voltage and test signal for 32 channels. Each card also acts as a patch panel for the differential output of 32 preamplifiers (placed at a maximum distance of 30 cm) which are grouped in a single twisted pair cable 30 m long reaching the counting room.

The shapers (each consisting of a hybrid circuit of 2.5×5 cm^2) and the ADCs are assembled on FASTBUS boards, each grouping 64 channels, for a total of 14 shaper and 14 ADC modules distributed in 3 FASTBUS crates. The shaper and ADC boards are interleaved within a crate and are connected by two 64 conductors flat cables 5 cm long.

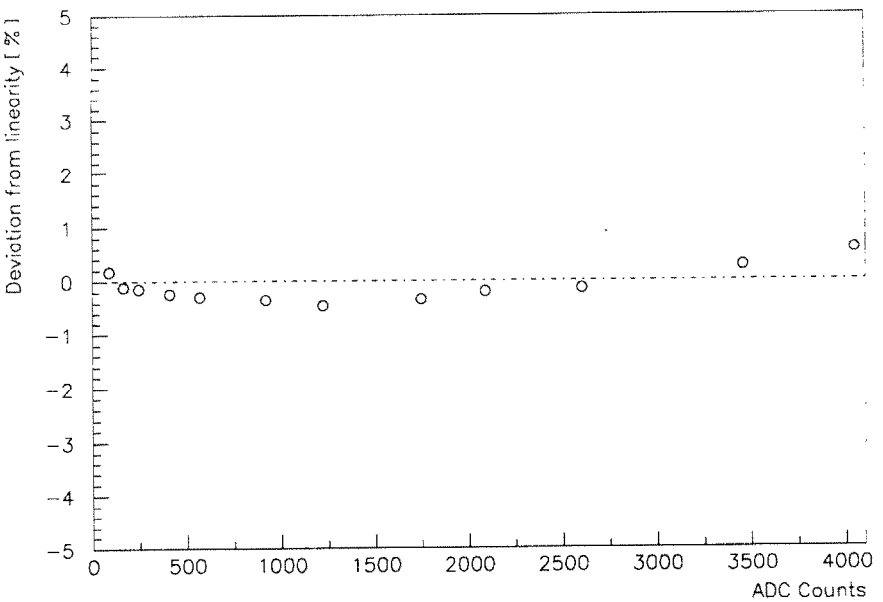

Fig. 16. Linearity of the electronic chain. The deviations from a straight-line fit are shown as a function of the ADC counts.

The preamplifier signal from the distribution cards are fed to the shaper boards through the module auxiliary connector placed in the rear of the crate.

5.5. Readout chain performance

5.5.1. Electronic noise and cross-talk

The performance of the charge preamplifier-shaper chain was tested, using 9 lead–glass counters assembled in a 3×3 structure (nonet), during several test beam runs at CERN. The equivalent noise charge (ENC) was measured with a 30 m long cable between the preamplifier and the shaper (the same cable length as used in the experiment). The results are plotted in Fig. 15 as a function of the supply voltage of the tetrode. At the operating voltage of 800 V the ENC average value was measured to be $344 \pm 34\ e^-$. The ENC is practically insensitive to the high voltage up to the maximum allowed value, if the bipolar output of the shaper is used.

In the operating conditions of the experiment, and for the whole sample of 875 channels, the average noise is estimated to be around 600 e^-, still within the requirements for the detector performance.

The electronic cross-talk of the whole calorimeter was measured both using the monitor LEDs, by pulsing one channel at a time, and the test signal, by pulsing 8 channels at a time. All the channels show a cross-talk level lower than 0.3%.

5.5.2. Linearity

The linearity of the preamplifier-shaper chain has been measured by pulsing with a test signal, whose amplitude was monitored by means of a digital LeCroy oscilloscope. The intrinsic uncertainty of such a method has been estimated to be about 1%. Fig. 16 shows the resulting deviation from linearity, measured over the energy region of interest. The deviation is within 1%, compatible with the accuracy of the measuring procedure.

5.6. Fast timing signal

A fast signal from a threshold discriminator was implemented on the shaper boards. The main purpose of this signal is to provide precise timing information and to reject energy depositions which are not associated with the event trigger. This signal can also be used to provide a trigger based on energy released in the calorimeter, if needed.

The output from the first stage of the shaper is strongly differentiated and fed to the input of a dual ECL discriminator (Analog Devices AM96687). A variable threshold is common to all the 64 channels in the board and the discriminator width is set to 3 μs. The 64 discriminator output signals are divided into four groups of 16 channels each which are connected in OR. The four signals so obtained are fed to a FASTBUS TDC (LeCroy 1876) which measures the time of both the leading and trailing edge with respect to a common stop provided by the event trigger. This is necessary to identify energy depositions occurring at different times in the same group of 16 channels in OR. The background event may occur earlier, in which case the leading edge of the OR signal arrives earlier with respect to the common stop. If the background event occurs later, the leading edge of the OR signal is in time but the width of the signal is larger since it is the OR of the event and the background signals.

Even in the absence of background events, the width of the timing signals, which is in principle the same (3 μs), may vary because of the tolerance of the R-C circuit components or of the different switching threshold of the latch enable input of different discriminators. As a consequence,

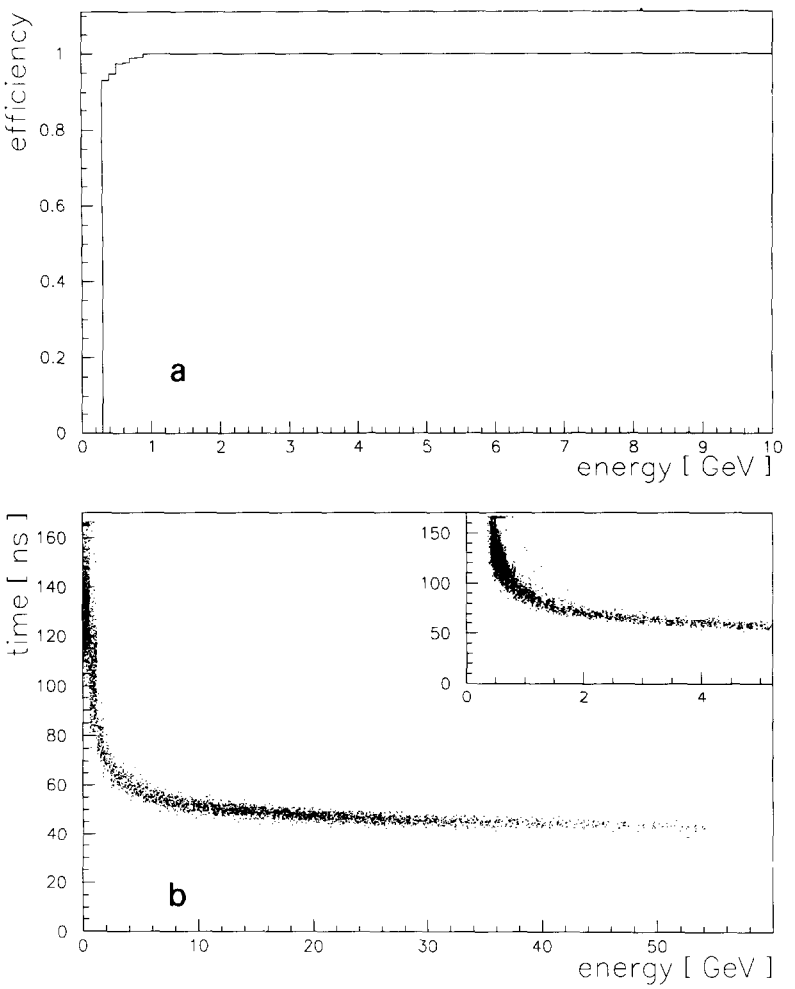

Fig. 17. (a) Trigger efficiency for a 10 mV threshold and (b) discriminator firing time vs. energy deposition.

the timing signal width for each channel must be accurately measured.

The timing resolution of the individual channel is of the order of a few nanoseconds.

The discriminator firing efficiency as a function of threshold and its time resolution were measured for two channels in a test beam from the CERN SPS. The firing efficiency is shown in Fig. 17a as a function of energy deposition for a threshold of 10 mV which is the lowest acceptable value. Fig. 17b shows the correlation between the discriminator firing time and the energy deposition, for all the 875 channels. After correcting for the time slewing, a resolution of the order of 1 ns is obtained for energy depositions above 10 GeV.

6. Detector performance

The NOMAD electromagnetic calorimeter has so far been in operation for more than a year. Its performance will be fully discussed in a forthcoming paper. In this section, a summary of the main results is given, with an emphasis on the aspects more closely related to the performance of the photodetectors and electronic chain.

The response uniformity as a function of the impact point might in principle be degraded by the strong photocathode non-uniformity induced by the magnetic field and by the counter geometry. However – at least for the diffused light generated by electrons and LEDs – the multiple reflections inside the lead–glass strongly reduce such an effect. As a consequence, no substantial deterioration of the response uniformity is observed in the presence of a magnetic field. In the operating conditions of the experiment the overall non-uniformity does not exceed 0.2%.

The response of the whole detector chain (lead–glass, PM and electronics), as measured in the X5 test beam of the SPS, is linear within $\pm 0.2\%$ in the energy range 10–80 GeV.

The photoelectron statistics – which provides the main contribution to the energy resolution for a lead–glass calorimeter – is not substantially spoiled by the partial photocathode blinding induced by the field and by the cut at 45° of the counter face. The good tetrode quantum efficiency

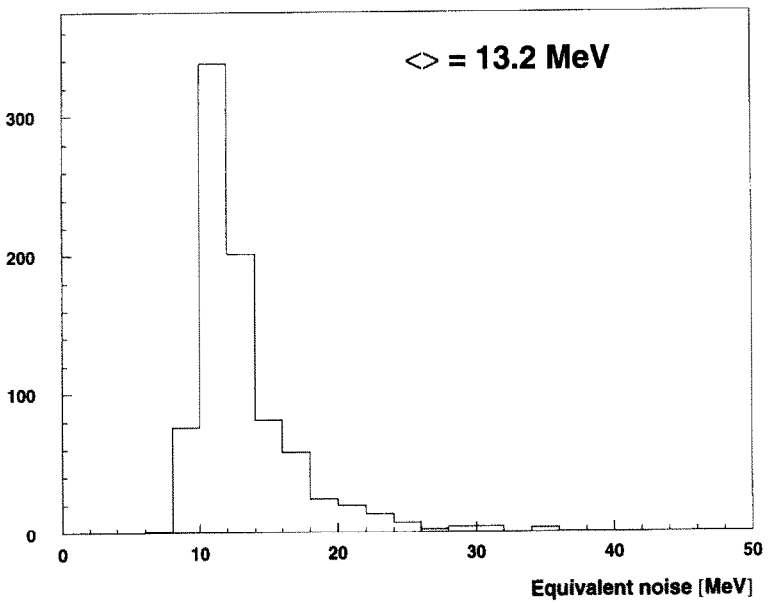

Fig. 18. The distribution of the equivalent noise for the full 875 counter sample.

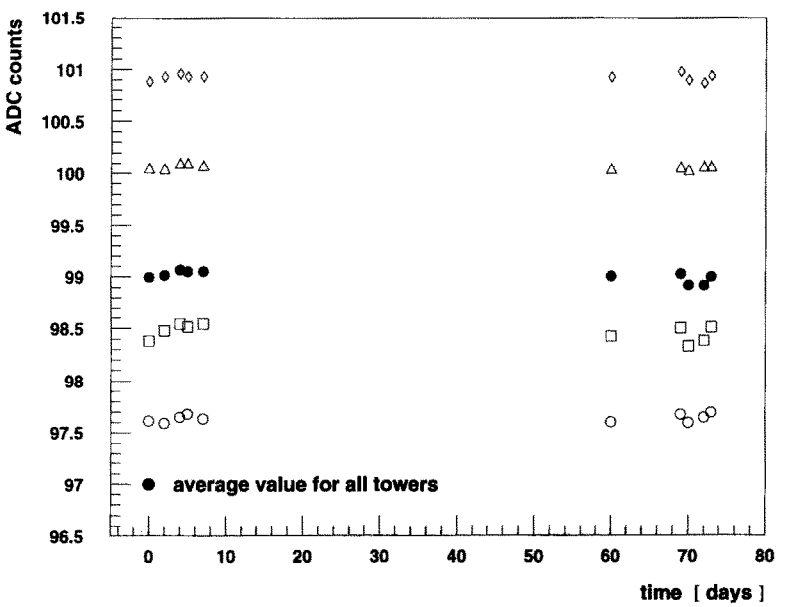

Fig. 19. Pedestal values vs. time for some individual channels and for the average of 875 calorimeter cells.

and optical coupling to the lead-glass result in an average yield of 1400 photoelectrons/GeV. The scaling term for the energy resolution is $\sim 2.7\%/\sqrt{E}$ from pure photoelectron statistics, increasing to $3.4\%/\sqrt{E}$ due to fluctuations in the release of energy and leakage. Such a value is not substantially affected by the operation in a magnetic field.

The photoelectron yield, together with the tetrode gain and the electronic noise, also determines the signal to noise ratio. To detect energy depositions below 100 MeV, which can be shared among different calorimeter cells, an equivalent noise of the order of 20 MeV in a single channel is needed. With an average of 1400 photoelectrons/GeV, a gain of 40, an effective noise in operation of about 600 e^-, the average equivalent noise is 10 MeV, well within the requirements. The equivalent noise distribution for all the 875 calorimeter channels is shown in Fig. 18.

The stability in response of the calorimeter has been monitored since the time of its installation in the NOMAD detector. The pedestals – whose values are not affected by the presence of the magnetic field – are found to be stable during the time of operation, as shown in Fig. 19. The response to electrons is being monitored on an assembly of 58 lead-

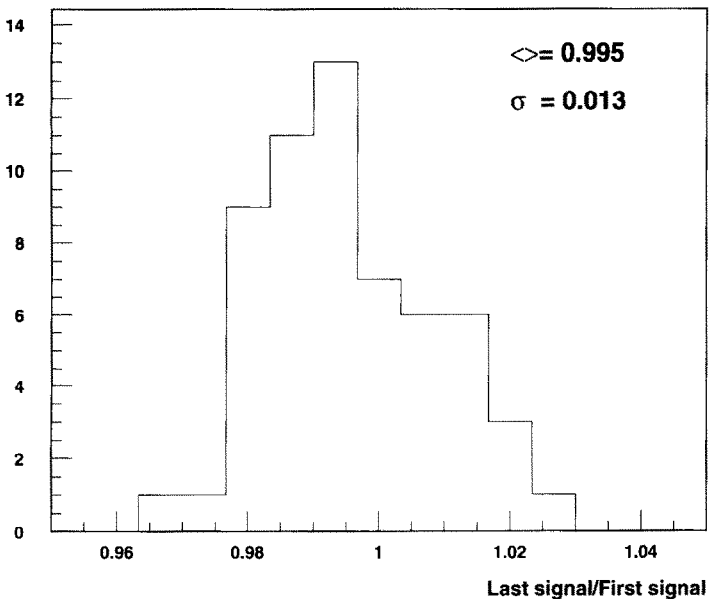

Fig. 20. Response variation for two electron calibrations of 58 lead-glass blocks, performed 22 months apart.

glass counters identical to the ones installed in the detector, repeatedly exposed to the X5 calibration beam of the SPS. The response stability over a period of 22 months is within 1%, as shown in Fig. 20.

7. Conclusions

In this paper results on the performance of the NOMAD electromagnetic calorimeter have been presented. With an appropriate choice of the counter geometry and of the light detector, the calorimeter can be operated in a magnetic field transverse to the counter axis, with excellent response uniformity, signal to noise ratio, and energy resolution. The detector has shown stability and reliability over a running period of more than one year.

Acknowledgements

The Italian groups are very grateful to Giorgio Goggi for his contribution in the setting up of their participation to the Nomad experiment.

The authors wish to thank the technical staff of the Cosenza, Firenze, Moscow, Padova, Pavia and Pisa groups for their invaluable contributions. Special thanks are due to A. Vicini for his continuous contribution to the mechanics and to D. Rizzi for his significant contribution in setting up part of the electronics.

Thanks are due to the CERN staff for their important contributions. We wish in particular to thank W. Huta and A. Beer for their constant help on the electronics, L. Camilleri for his collaboration during test-beam measurements and finally A. Rubbia for his help in part of the analysis.

The financial support of INFN and INR is gratefully acknowledged.

References

[1] NOMAD Collaboration, CERN-SPSLC/91-21; CERN-SPSLC/91-48; CERN-SPSLC/91-53; CERN-SPSLC/93-19; CERN-SPSLC/94-21; CERN-SPSLC/94-28.
[2] NOMAD Collaboration, CERN-SPSLC/93-31.
[3] Industry for Optical Glass, Moscow, Russia.
[4] M.D. Rousseau et al., IEEE Trans. Nucl. Sci. NS-30 (1983) 479.
[5] M. Akrawy et al., Nucl. Instr. and Meth. A 290 (1990) 76.
[6] P. Checchia et al., Nucl. Instr. and Meth. A 248 (1986) 317.
[7] P. Checchia et al., Nucl. Instr. and Meth. A 275 (1989) 49.
[8] F. Binon et al., Nucl. Instr. and Meth. A 248 (1986) 86.
[9] D. Autiero et al., A high stability light emitting diode system for monitoring lead-glass electromagnetic calorimeters, submitted to Nucl. Instr. and Meth.
[10] G. Barichello et al., Nucl. Instr. and Meth. A 254 (1987) 111.
[11] I. Lippi et al., Nucl. Instr. and Meth. A 286 (1990) 243.